

Electronic Supporting Information for

**High-Strength 3D Printed Poly(lactic acid) Composites Reinforced by Shear-Aligned
Polymer-Grafted Cellulose Nanofibrils**

*Peter V Kelly¹, S. Shams Es-haghi^{2,3}, Ahmad A. L. Ahmad^{1,3}, Meghan E Lamm⁴, Katie
Copenhaver⁴, Elif Alyamac-Seydibeyoglu,^{3,5} Soydan Ozcan⁴, Douglas J Gardner^{3,6}, William M
Gramlich^{1,3*}*

¹Department of Chemistry, University of Maine, Orono, ME 04469

**²Department of Chemical and Biomedical Engineering, University of Maine, Orono, ME
04469**

³Advanced Structures and Composites Center, University of Maine, Orono, ME 04469

⁴Manufacturing Science Division, Oak Ridge National Laboratory, Oak Ridge, TN 37748

⁵Department of Chemical Engineering, Ege University, 35100 Izmir, Turkey

⁶School of Forest Resources, University of Maine, Orono, ME 04469

***Corresponding author:** william.gramlich@maine.edu

Synthesis and Scale-Up

Methacrylated Cellulose Nanofibrils (MetCNFs)

Batches of 0.5 kg CNFs on a dry basis were dispersed to 0.5 wt.% with reverse osmosis (RO) water in a 100 L jacketed glass reactor purchased from Chemglass Life Sciences (Vineland, NJ). Methacrylic anhydride was added to reach a final concentration of 0.6 M, at which point the reaction was titrated with 10 M NaOH for 2 hours, keeping the suspension pH between 9 and 11. Upon completion of the reaction the suspension was filtered using a W.M. Watermark (Holland, MI) 320 mm filter press, with subsequent resuspension in RO water and filtration cycles being performed until FTIR analysis of MetCNF aliquots showed no change in the bands associated with the surface methacrylate at 1720 cm^{-1} or any side products. In total about five washes were required to purify the product.

Polymer-Grafted Cellulose Nanofibrils

Three batches of each synthesis were performed to achieve the amount of material required for compounding and 3D printing. The PMAM-MetCNF syntheses were carried out with a monomer concentration of 88 mM, in 0.5 wt.% MetCNF suspensions with approximately 60 L of total volume. The suspensions were sparged for 90 minutes with N_2 and heated to $70\text{ }^\circ\text{C}$ using a Huber (Offenburg, Germany) Unistat 410 temperature control system attached to the reactor's glass jacket. A 0.129 M KPS stock solution was added to reach a final initiator concentration of 10 mM. The PNIPAM-MetCNF syntheses were performed with the same monomer concentration, MetCNF solids content, and total reaction volume as the PMAM-MetCNF scale up but were performed at room temperature using a redox initiator system instead of KPS. After 90 min of sparging with nitrogen, 0.6 M APS and TEMED stock solutions were added to achieve final

concentrations of 9.6 mM. Both sets of reactions were run for 3 hours at which point the suspensions were collected and purified via subsequent RO water washing cycles using the W.M. Watermark (MI, USA) 320 mm filter press with a capacity of 0.3 ft³. FTIR aliquots were taken after each wash to verify when unattached homopolymer was fully removed, which took about three washes.

ATR-FTIR Suspension Characterization

Suspensions were freeze-dried prior to analysis and scanned from 4000 cm⁻¹ to 450 cm⁻¹ with a resolution of 4 cm⁻¹ using a Perkins Elmer (Waltham, MA) Spectrum Two. The instrument averaged 8 scans which were then worked up using an ATR correction, manual baselining, and normalization to the 1055 cm⁻¹ band as previously reported [1].

Spray Drying of CNFs and Powder Characterization

Suspensions were diluted to 1 wt.% and sprayed onto a spinning disk atomizer operating at 30,000 RPM with an inlet gas temperature of 235 °C and an outlet temperature of approximately 120 °C. Dried powder was collected from the cyclone filter.

Imaging of the spray dried reinforcements was done using a Cube-II tabletop SEM (EmCrafts Co. Ltd. Hanam, South Korea). Samples were dispersed over graphite tape and sputter coated with 6 nm of Au/Pd alloy (60:40) to facilitate imaging. An acceleration voltage of 10 kV and a working distance of approximately 10 mm was used.

Particle size distributions were assessed using a Morphologi G3 from Malvern PANalytical (Westborough, Massachusetts). Automated optical microscopy measurements were taken of dispersed powdered samples at 5x and 20x magnifications with circular equivalent diameters calculated from particle areas and collated by the analysis software.

Statistical Treatment of Tensile Data

Using the experimental data sets collected, 95% confidence intervals were calculated using the student's t -statistic for a two-tailed distribution. Two-tailed t -tests assuming unequal variance were conducted to determine the statistical significance of the differences observed between samples. The chosen significance level ($\alpha = 0.5$) was adjusted using the Bonferroni correction to avoid Type I errors appearing in the analysis of multiple groups [2]. As such the P-values calculated from the t -tests were deemed significant if they fell above the corrected significance level, $\alpha = 0.000757$.

Determination of Reinforcement Loading for Pilot Scale Testing

To assess the possible reinforcement loading levels for subsequent extrusion and additive manufacturing trials, small-scale batch melt mixing of the materials in PLA was performed. The tensile data shown in **Figure S2** (full data in **Table S2** and representative curves in **Figure S3**) demonstrated that both the PNIPAM and PMAM modified CNFs increased strength and stiffness more effectively than the SD CNF controls with the largest improvements seen at the 20 wt.% loading levels. As commonly seen in fiber-reinforced composites, the strain at break of the materials decreased with higher loading levels as the samples became more brittle [3]. At the 20 wt.% loading level the SD CNFs exhibited decreased tensile strength relative to neat PLA, presumably by introducing defect sites where stress concentrations lead to crack formation [4]. The polymer-grafted MetCNFs increased strength as a function of loading, presumably because their more fibrillar architecture and better dispersion led to more effective network formation. The PNIPAM-MetCNF composite at 20 wt.% achieved a tensile strength of 71.5 ± 1.9 MPa and a tensile modulus of 5.6 ± 0.2 GPa, improvements of 22% and 39% over the corresponding SD CNF

control respectively. The PMAM-MetCNF composite exhibited more modest improvements, with 13% and 12% improvements in tensile strength and tensile modulus, respectively, at 20 wt.%. These data are in general agreement with our previously published work using small-scale synthesis and spray drying. The major differences being that the spray-dried polymer modified CNFs in that work displayed a more fibrillar morphology and the PNIPAM-MetCNF composites achieved optimal loading at 10 wt.% with a decrease in strength at higher loadings [5]. This deviation in optimal loading could be the result of the morphological change or could be due to the lower degree of polymer functionalization seen in the pilot-scale synthesis.

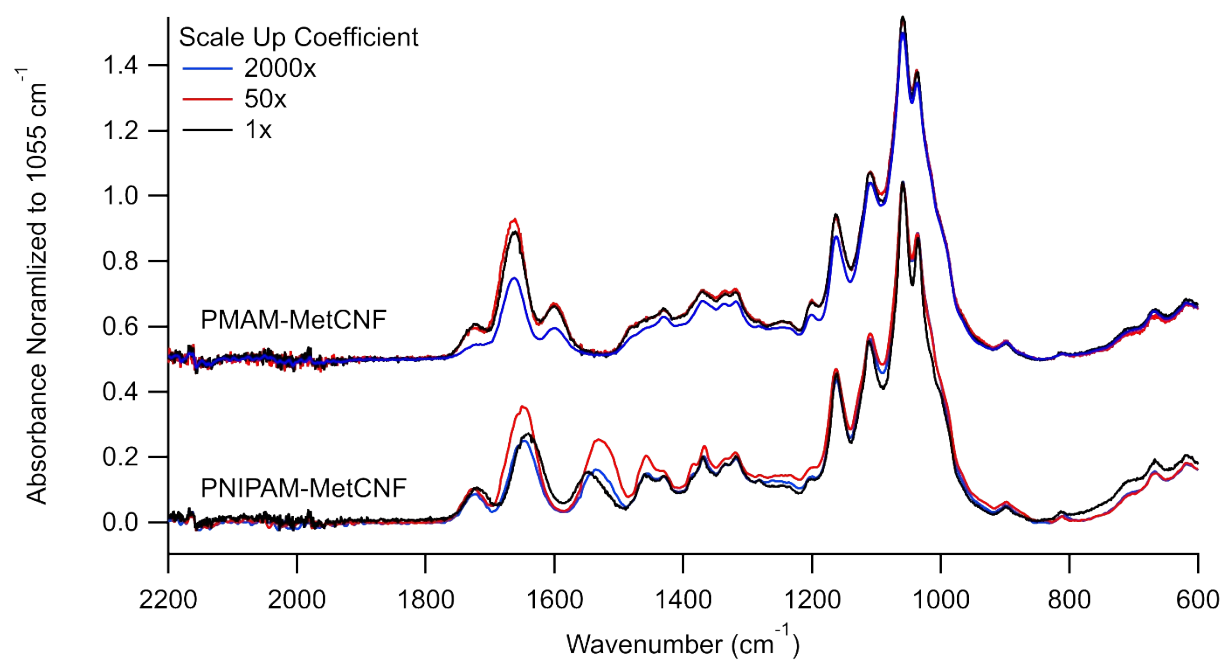


Figure S1. ATR-FTIR Characterization PNIPAM-MetCNF and PMAM-MetCNF syntheses at different scale multipliers starting with a previously published 0.15 g scale synthesis (1x).¹ Curves shifted vertically to improve clarity.

Table S1. Morphological Analysis of Spray Dried Powders.

Sample	D[n,0.1] (μm) ^a	D[n,0.5] (μm)	D[n,0.9] (μm)	D avg (μm) ^b	D[v,0.1] (μm) ^c	D[v,0.5] (μm)	D[v,0.9] (μm)	D[4,3] (μm) ^d
SD CNF	0.60	2.04	14.08	5.12	16.36	39.56	92.15	51.69
PNIPAM	0.60	2.40	19.89	6.96	22.49	47.32	94.58	54.11
PMAM	0.72	5.18	15.15	7.31	16.9	56.86	201.6	89.23

^a The D[n,x] values represent the maximum particle diameter for the xth percentile of the particles by number. ^b The number average mean particle diameter. ^c The D[v,x] values represent the maximum particle diameter for the xth percentile of the particles by volume. ^d The volume average mean particle diameter.

Table S2. Tensile properties of composites from small-scale batch melt mixing of GEA Niro spray dried CNFs.

Sample	n	Tensile Strength (MPa)^a	Tensile Modulus (GPa)^a	Elongation at Break (%)^a
SD CNF 5%	9	62.6 ± 0.5	3.7 ± 0.1	4.3 ± 0.3
SD CNF 10%	6	62.1 ± 0.7	3.8 ± 0.1	3.7 ± 0.2
SD CNF 20%	5	58.7 ± 0.6	4.0 ± 0.2	3.4 ± 0.6
PMAM 5%	5	64.0 ± 0.8	3.8 ± 0.1	4.2 ± 0.6
PMAM 10%	6	63.4 ± 1.5	3.9 ± 0.2	4.1 ± 0.3
PMAM 20%	10	66.4 ± 2.1	4.5 ± 0.1	3.9 ± 0.4
PNIPAM 5%	7	65.5 ± 1.4	3.9 ± 0.2	3.6 ± 0.2
PNIPAM 10%	9	67.6 ± 3.3	4.5 ± 0.2	3.7 ± 0.4
PNIPAM 20%	4	71.5 ± 3.7	5.6 ± 0.8	3.3 ± 0.3

^a Average tensile property ± 95% confidence intervals.

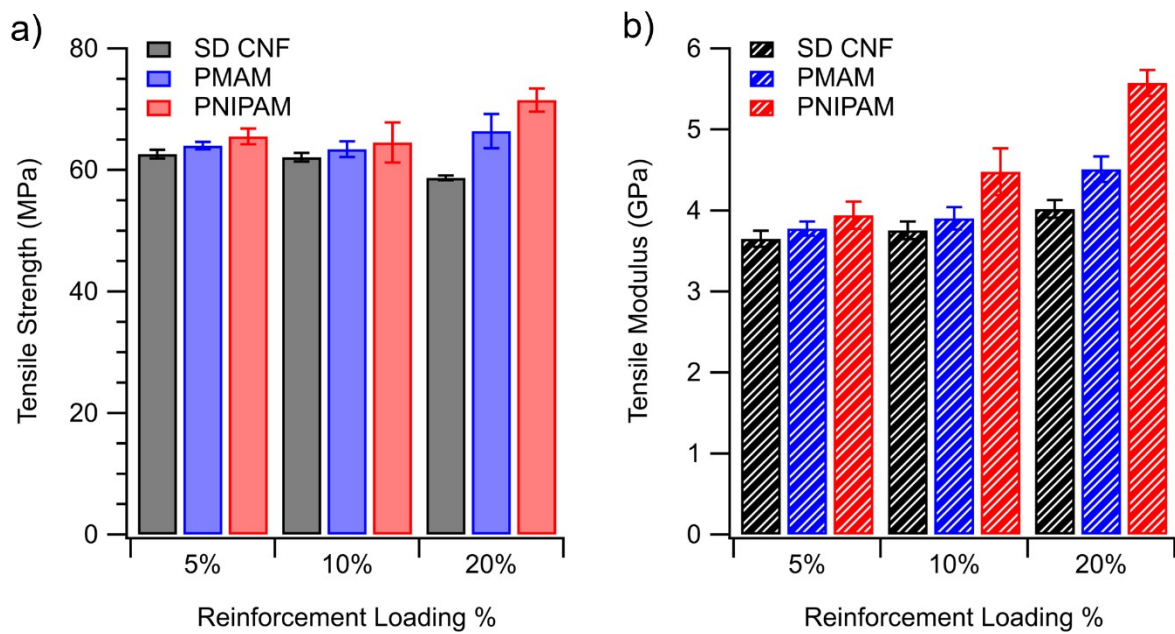


Figure S2. a) Tensile strength and b) tensile modulus of pilot-scale spray-dried reinforced PLA composites at different loading levels produced by small-scale batch melt mixing and compression molding.

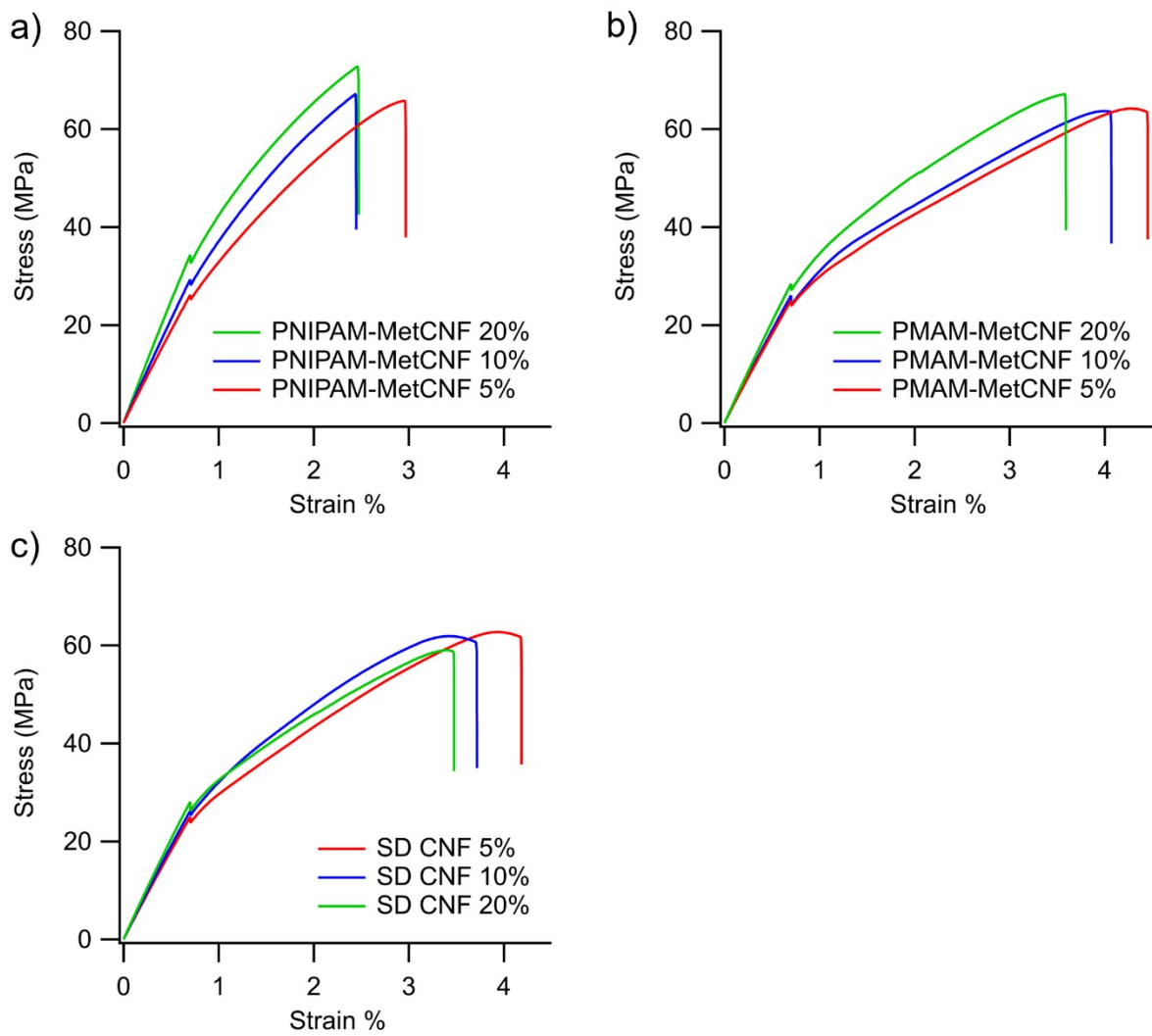


Figure S3. Representative tensile curves from small-scale batch melt mixing of GEA Niro spray dried a) PNIPAM-MetCNFs, b) PMAM-MetCNFs, and c) unmodified SD CNFs in PLA.

Table S3. Thermal properties of 3D printing pellets and tensile bars.

Sample	X_c (%)	T_g (°C)	T_{cc} (°C)	T_m (°C)
PLA Pellets	41.5	54.9	97.6	145.6
20% SD CNF Pellets	1.5	56.8	99.6	142.9
20% PNIPAM Pellets	2.5	56.0	99.1	143.3
20% PMAM Pellets	0.0	57.6	102.0	144.4
PLA Printed	0.2	54.6	101.4	143.0
20% SD CNF Printed	0.2	53.0	87.95	139.7
20% PNIPAM Printed	4.0	58.5	104.1	145.7
20% PMAM Printed	3.7	54.2	89.7	147.6
PLA Compression	1.0	53.6	93.8	142.8
20% SD CNF Compression	2.2	52.3	86.7	139.3
20% PNIPAM Compression	0.0	53.9	92.6	141.4
20% PMAM Compression	2.7	51.4	84.10	138.2

Percent crystallinity (X_c) of the printing pellets and printed samples obtained from the first heating cycle. Onset temperature of glass transition (T_g), cold crystallization (T_{cc}), and melting (T_m) obtained from the second heating cycle to be more indicative of fibril-matrix interactions.

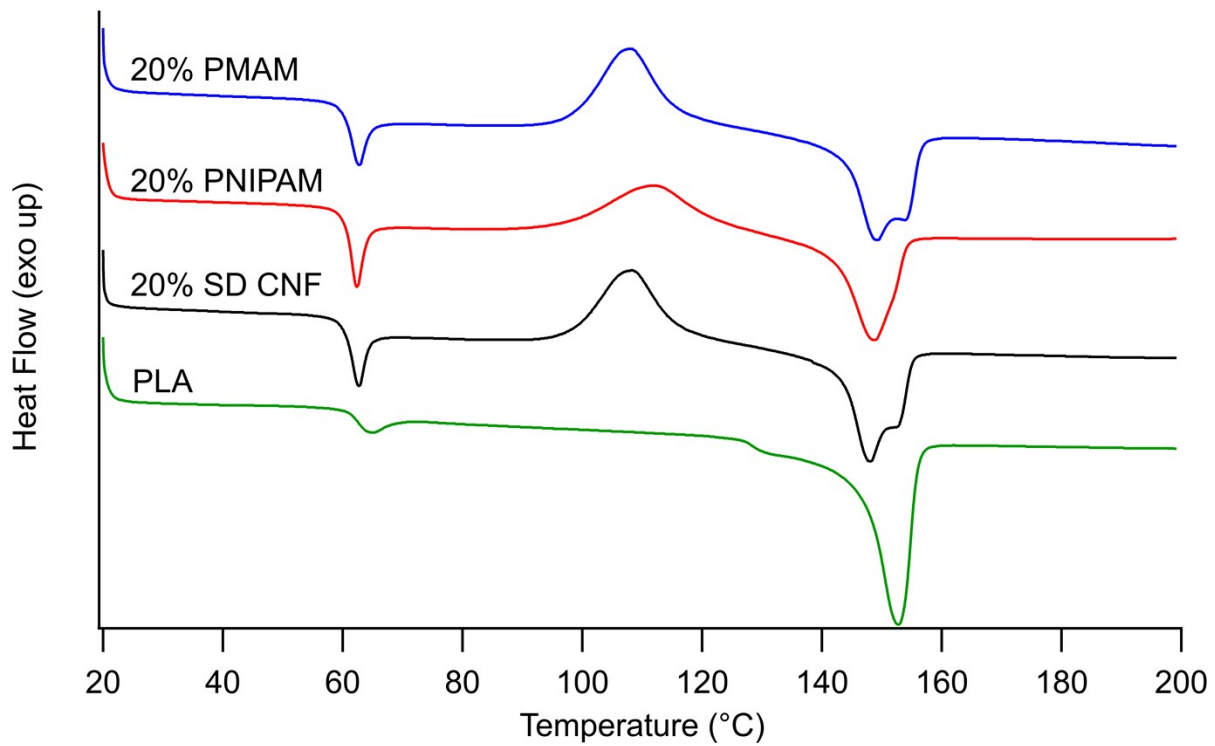


Figure S4. DSC curves from the first heating cycle of the extruded pellets used for printing and compression molding. The thermal transitions from left to right are the glass transition, cold crystallization, and melting. The melting transitions that included CNF reinforcements demonstrated two melting peaks belonging to the metastable α' -crystal and the stable α -crystal [6]

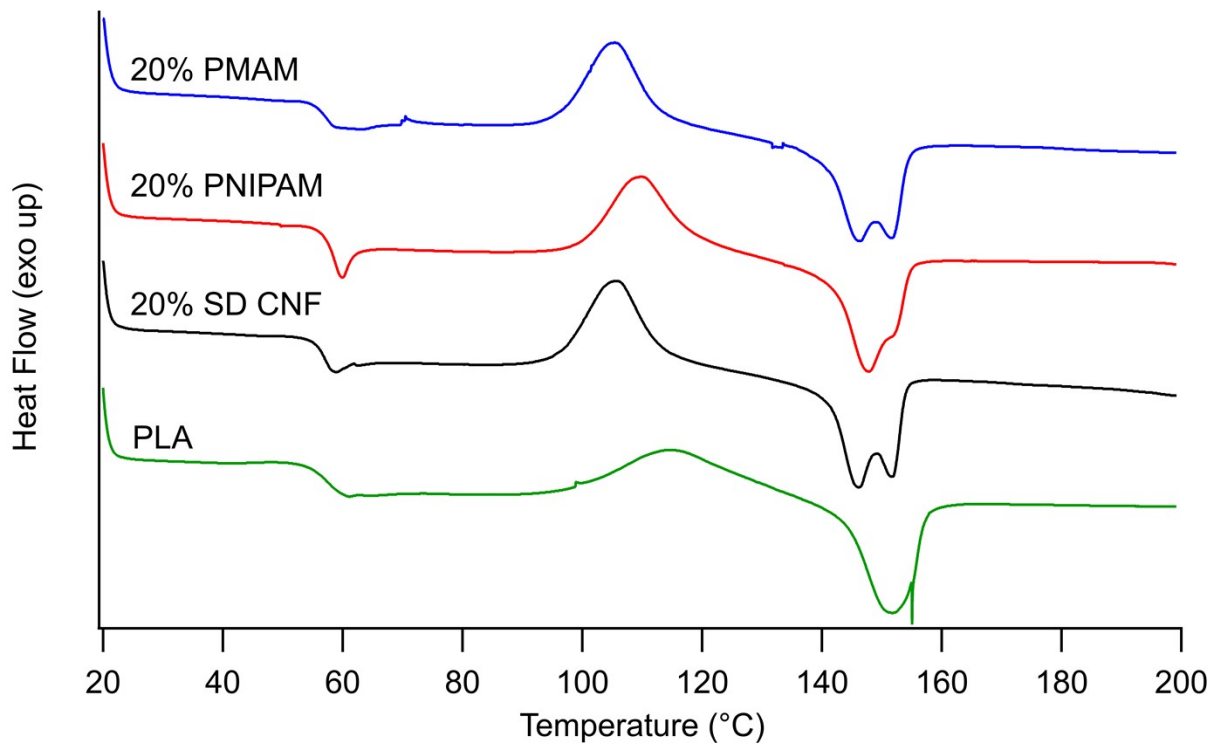


Figure S5. DSC curves from the first heating cycle of the compression molded tensile bars. The thermal transitions from left to right are the glass transition, cold crystallization, and melting. The melting transitions that included CNF reinforcements demonstrated two melting peaks belonging to the metastable α' -crystal and the stable α -crystal [6].

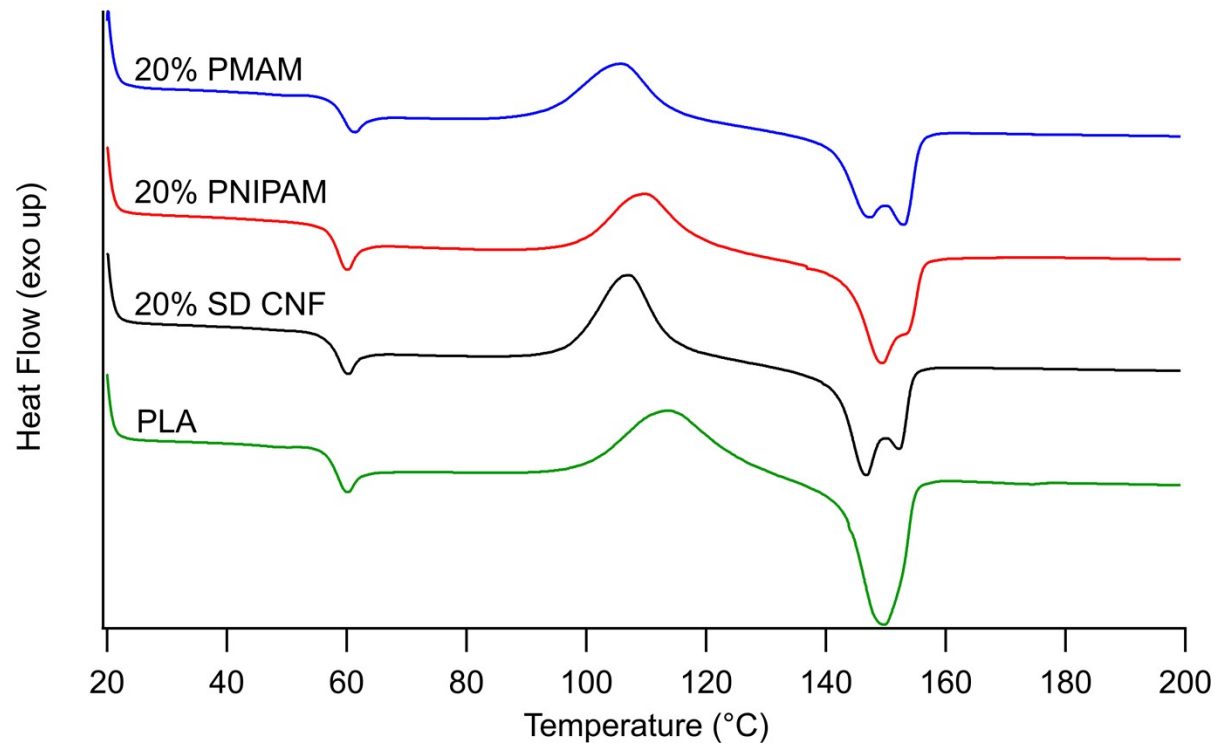


Figure S6. DSC curves from the first heating cycle of the 3D printed composite samples. The thermal transitions from left to right are the glass transition, cold crystallization, and melting. The melting transitions that included CNF reinforcements demonstrated two melting peaks belonging to the metastable α' -crystal and the stable α -crystal [6].

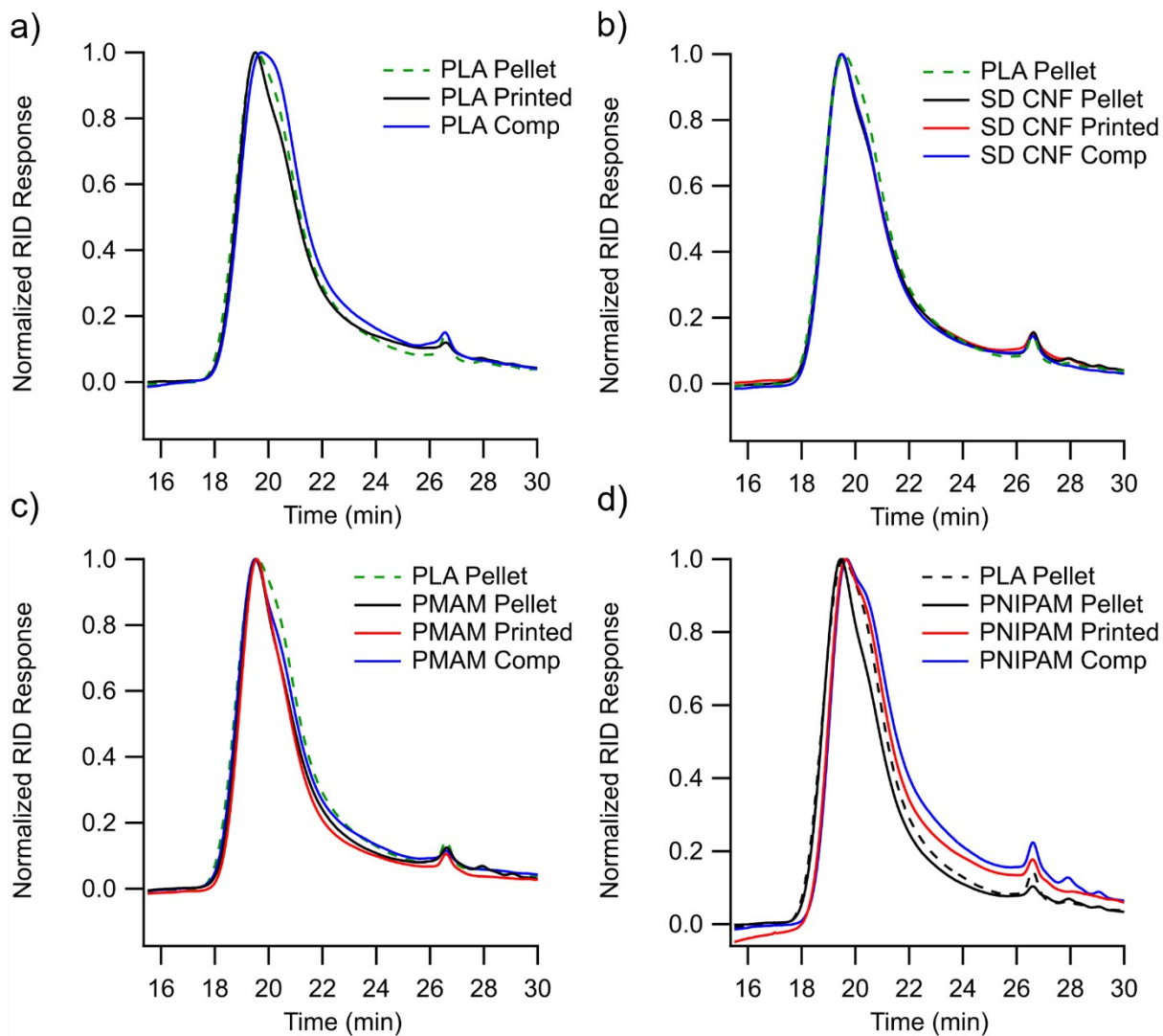


Figure S7. SEC elution curves of the PLA matrices from the a) extruded pellets, b) printed composite samples, and c) compression molded controls either neat or compounded with polymer-modified CNFs or the SD CNFs.



Figure S8. Photographs of FDM printed triangular prisms produced from the three composite materials and neat PLA showing good dimensional stability throughout the prints.

Table S4. Tensile properties of 3D printed parts machined into x-directional and z-directional tensile bars along with compression molded anisotropic controls.

Sample	N	Tensile Strength (MPa)^a	Tensile Modulus (GPa)^a	Elongation at Break (%)^a
Neat PLA X	9	62 ± 1.0	3.6 ± 0.5	5.5 ± 0.5
Neat PLA Z	9	57.5 ± 2.1	3.4 ± 0.2	4.0 ± 0.5
Neat PLA Compression	8	63.2 ± 0.7	3.6 ± 0.2	5.4 ± 0.3
SD CNF 20% X	9	52.2 ± 1.8	3.9 ± 0.1	3.2 ± 0.3
SD CNF 20% Z	6	44.5 ± 2.5	3.4 ± 0.2	3.2 ± 0.4
SD CNF Compression	9	58.2 ± 0.7	4.0 ± 0.1	3.9 ± 0.2
PNIPAM 20% X	9	87.9 ± 2.8	7.8 ± 1.3	2.8 ± 0.3
PNIPAM 20% Z	8	30.9 ± 2.7	5.1 ± 1.1	0.9 ± 0.3
PNIPAM 20% Compression	5	72.4 ± 3.4	5.6 ± 0.4	2.3 ± 0.4
PMAM 20% X	8	61.4 ± 1.7	4.5 ± 0.3	3.5 ± 0.3
PMAM 20% Z	5	47.4 ± 2.7	3.7 ± 0.2	2.9 ± 0.4
PMAM 20% Compression	8	63.1 ± 0.9	4.4 ± 0.5	3.9 ± 0.2

^a Average tensile property ± 95% confidence intervals.

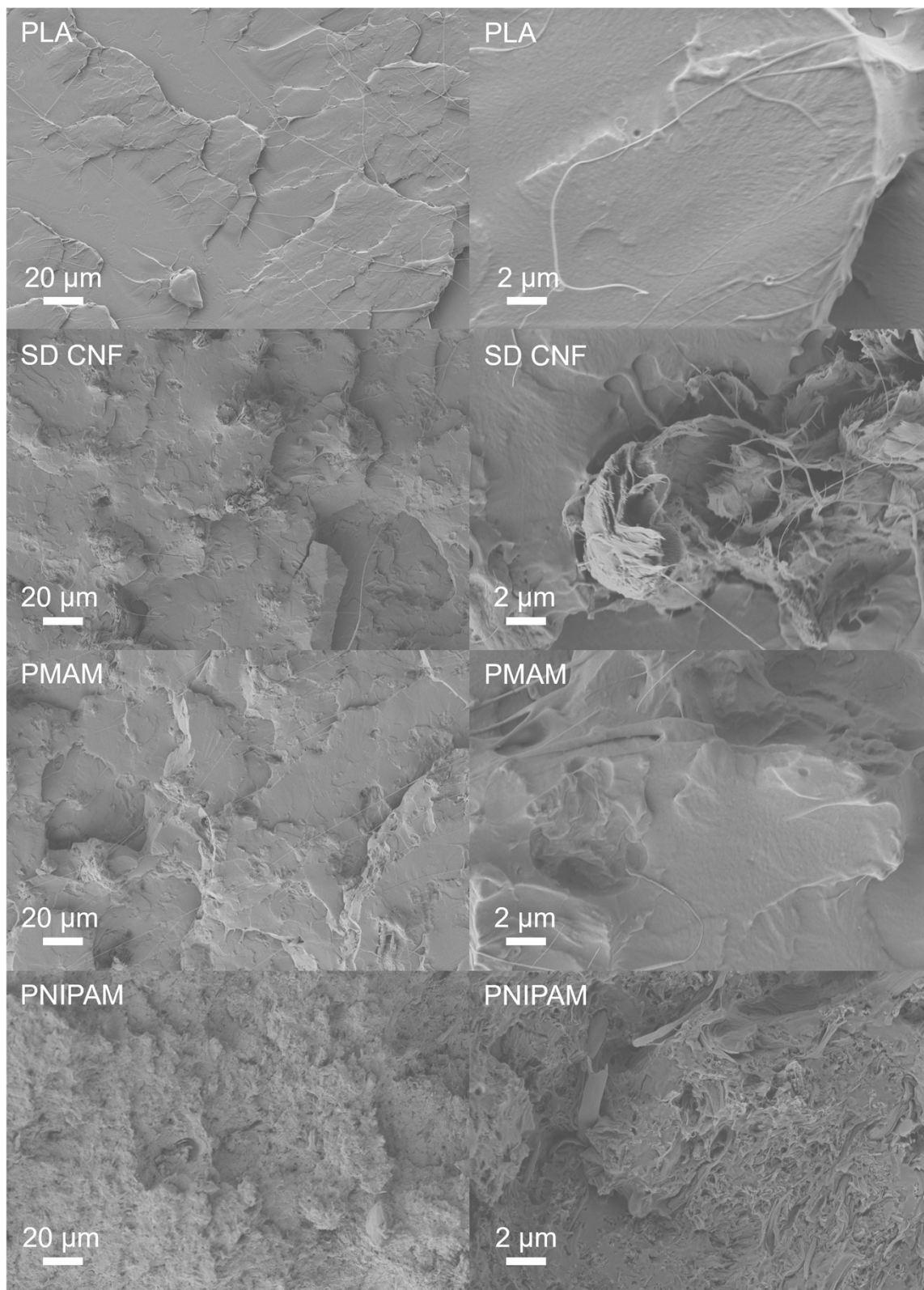


Figure S9. SEM images of fracture surfaces from the compression molded tensile bars made from the extruded pellets used in printing at 500x (left) and 5000x (right) magnifications.

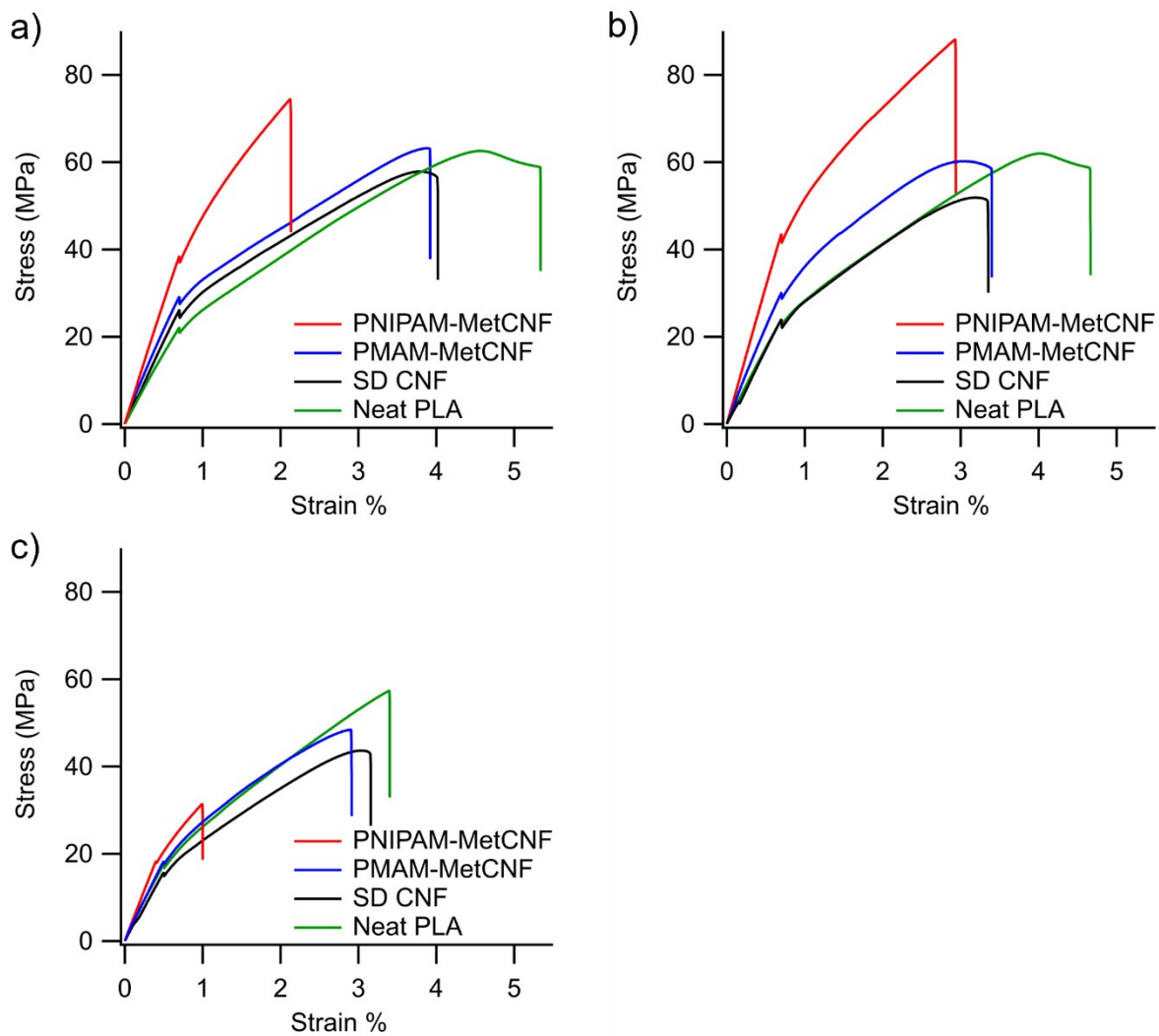


Figure S10. Representative tensile curves from a) compression molded isotropic controls, b) x-directional printed samples, and c) z-directional printed samples.

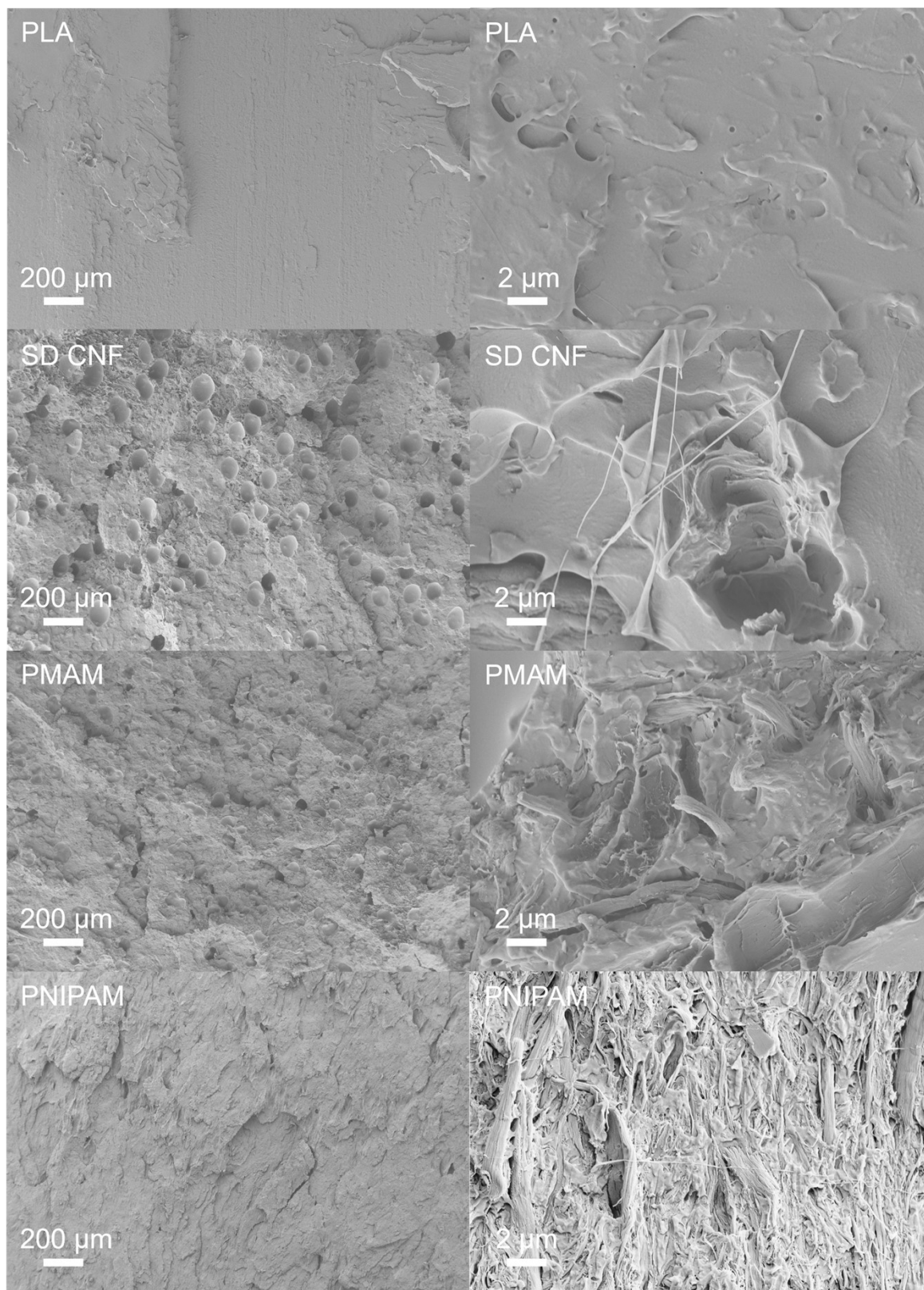


Figure S11. SEM images of fracture surfaces from the z-directional tensile bars at 500x and 5000x magnifications.

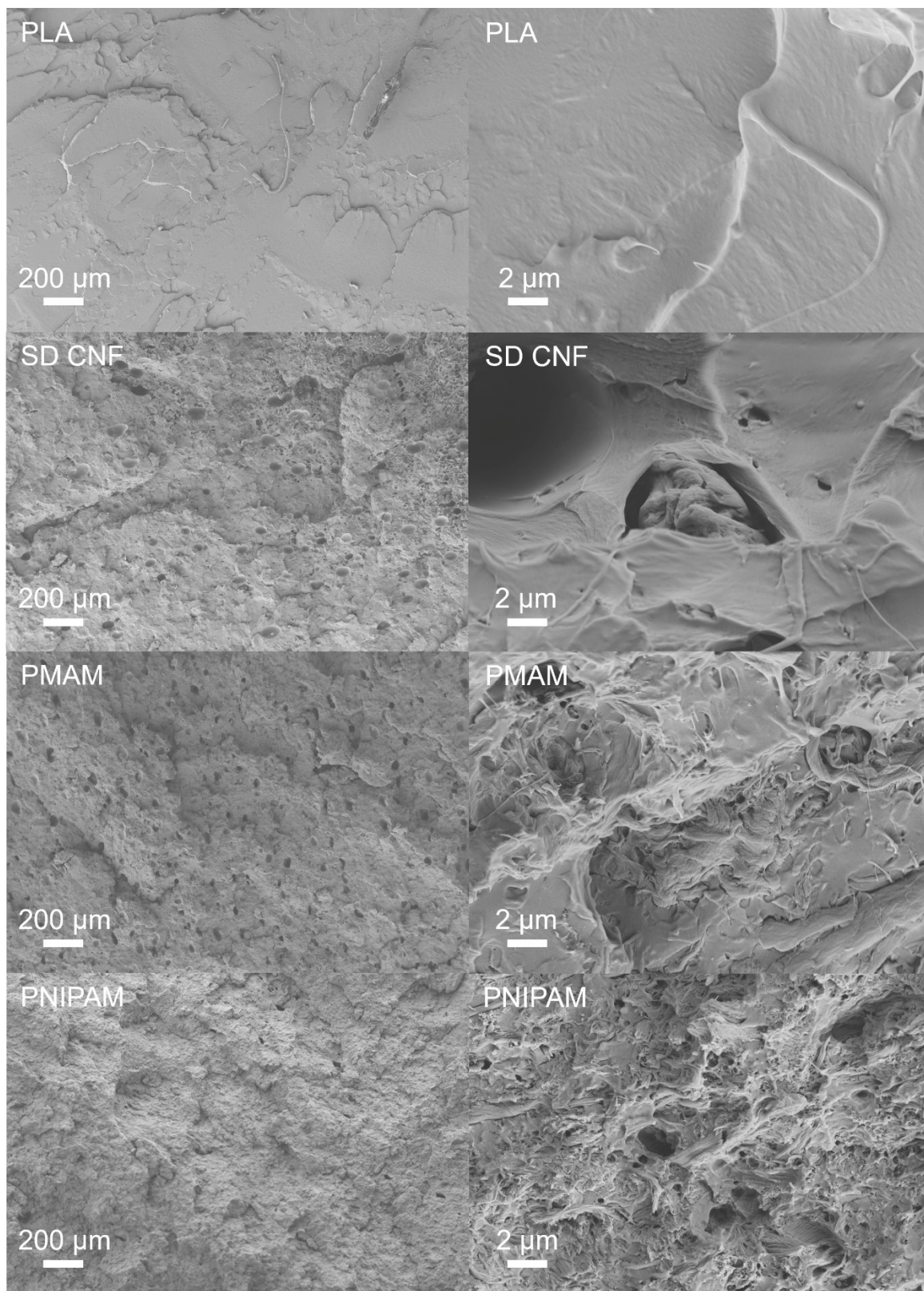


Figure S12. SEM images of fracture surfaces from the x-directional tensile bars at 50x and 5000x magnifications.

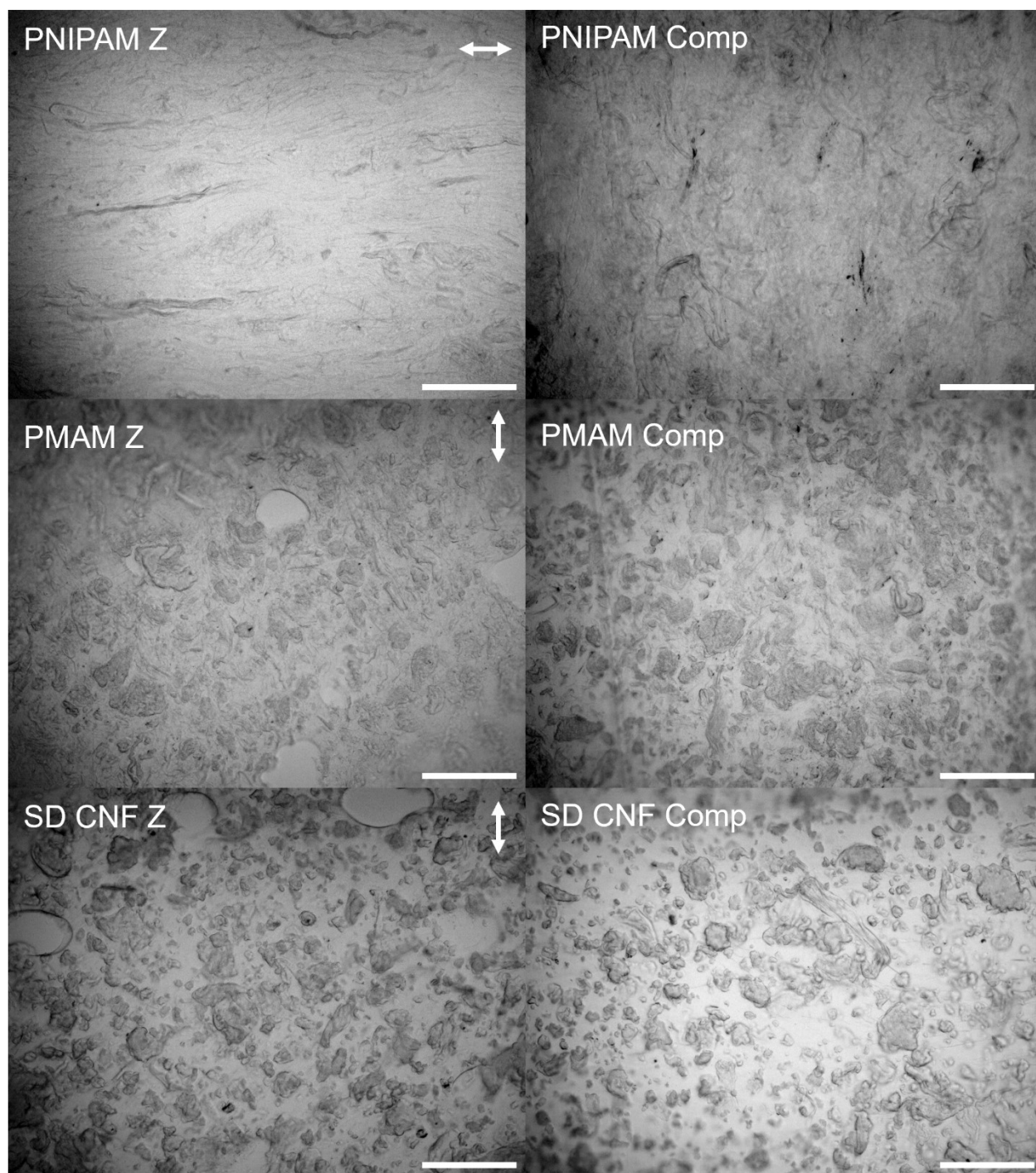


Figure S13. Optical microscopy images of 20 μm thick microtomed PLA composite samples reinforced with PNIPAM-MetCNFs, PMAM-MetCNFs, and SD CNFs at 20x magnification. Images on the left are from printed composites with the direction of printing denoted by the white arrow in the upper right corner. Images on the right are from compression molded composites. Scale bar on all images represents 100 μm .

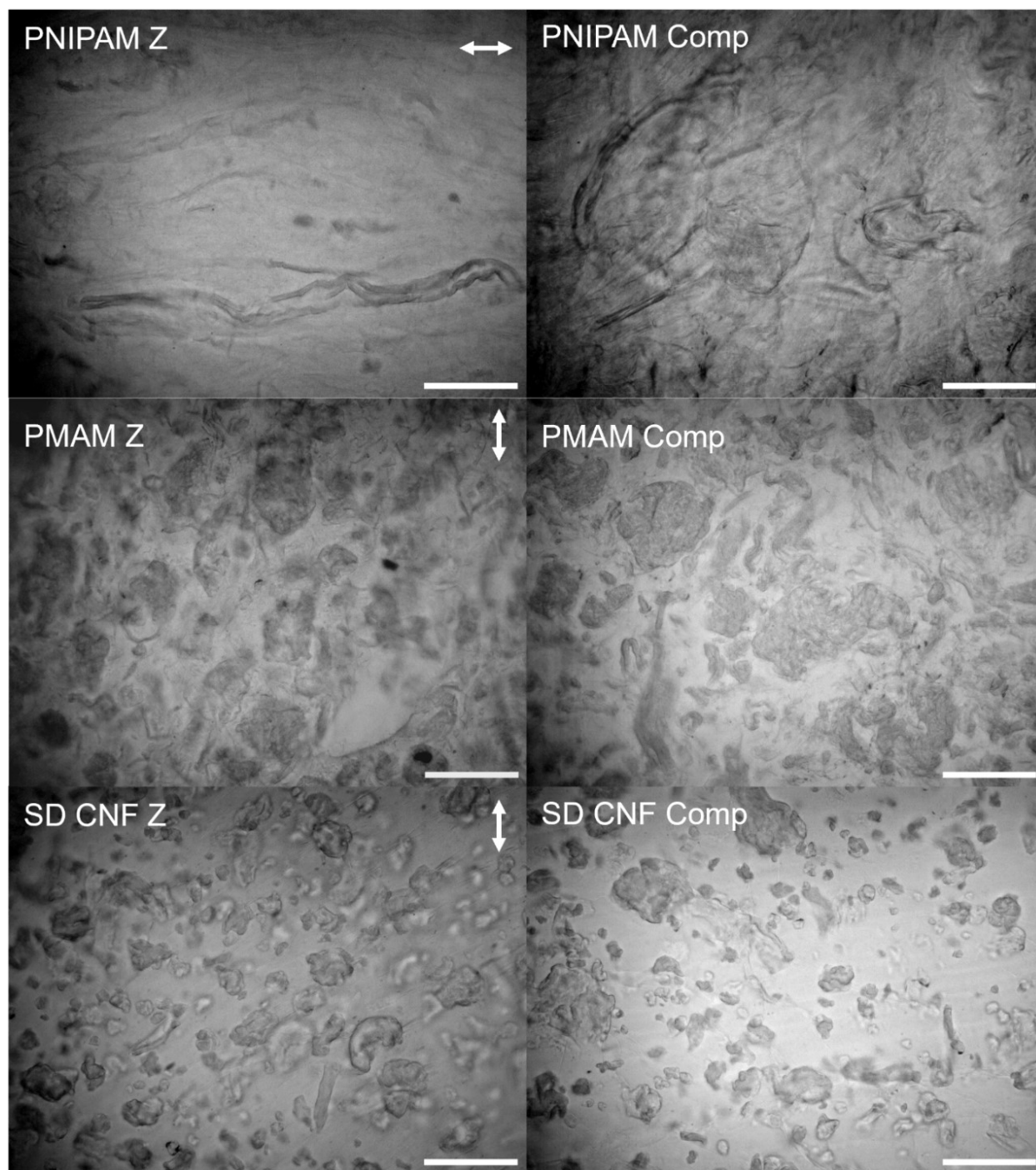


Figure S14. Optical microscopy images of 20 μm thick microtomed PLA composite samples reinforced with PNIAM-MetCNFs, PMAM-MetCNFs, and SD CNFs at 40x magnification. Images on the left are from printed composites with the direction of printing (z-direction) denoted by the white arrow in the upper right corner. Images on the right are from compression molded composites (Comp). Scale bar on all images represents 50 μm .

Table S7. Order parameters of composite samples calculated from polarized light microscopy measurements

Sample	Order Parameter S
SD CNF 20% Z	-0.03 ± 0.01
SD CNF Compression	0.02 ± 0.02
PMAM 20% Z	0.04 ± 0.02
PMAM 20% Compression	-0.01 ± 0.01
PNIPAM 20% Z	0.2 ± 0.01
PNIPAM 20% Compression	0.08 ± 0.02

Table S8. DMA dynamic moduli data of printed composites and isotropic control samples in the glassy and rubbery regions

Sample	Glassy Region (30 °C)		Rubbery Region (85 °C)	
	G' (MPa)	G'' (MPa)	G' (MPa)	G'' (MPa)
Neat PLA X	3032 ± 148	30 ± 2	3.9 ± 0.1	0.7 ± 0.01
Neat PLA Z	2862 ± 63	28 ± 1	3.9 ± 0.1	0.7 ± 0.04
Neat PLA Compression	2356 ± 102	24 ± 2	2.9 ± 0.1	0.6 ± 0.04
SD CNF 20% X	3039 ± 116	43 ± 2	9.0 ± 0.1	1.6 ± 0.01
SD CNF 20% Z	3320 ± 116	45 ± 3	9.8 ± 0.4	1.7 ± 0.1
SD CNF Compression	2762 ± 10	38 ± 1	7.7 ± 0.1	1.4 ± 0.01
PNIPAM 20% X	5072 ± 149	56 ± 1	245 ± 23	33 ± 3
PNIPAM 20% Z	3604 ± 22	38 ± 1	40 ± 2	8.0 ± 0.3
PNIPAM 20% Compression	3784 ± 248	42 ± 3	121 ± 6	18 ± 2
PMAM 20% X	3670 ± 127	47 ± 2	30 ± 1	4.8 ± 0.2
PMAM 20% Z	3039 ± 116	43 ± 2	9.0 ± 0.1	1.6 ± 0.01
PMAM 20% Compression	3051 ± 241	40 ± 3	20 ± 1	3.7 ± 0.2

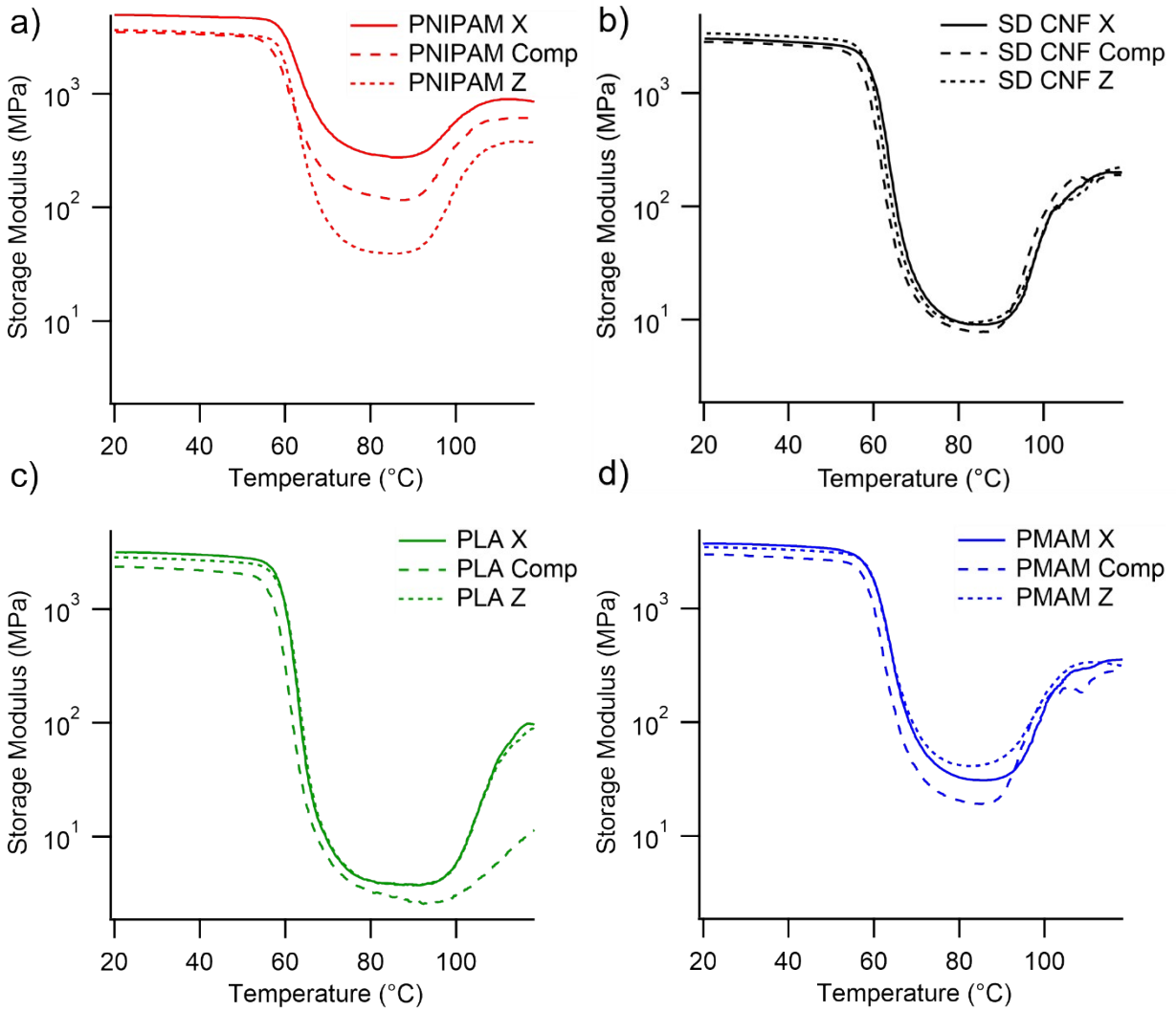


Figure S14. Storage moduli of a) PNIPAM-MetCNF, b) SD CNF, c) neat PLA, and d) PMAM-MetCNF composites in both printing directions and compression molded as a function of temperature measured by DMA.

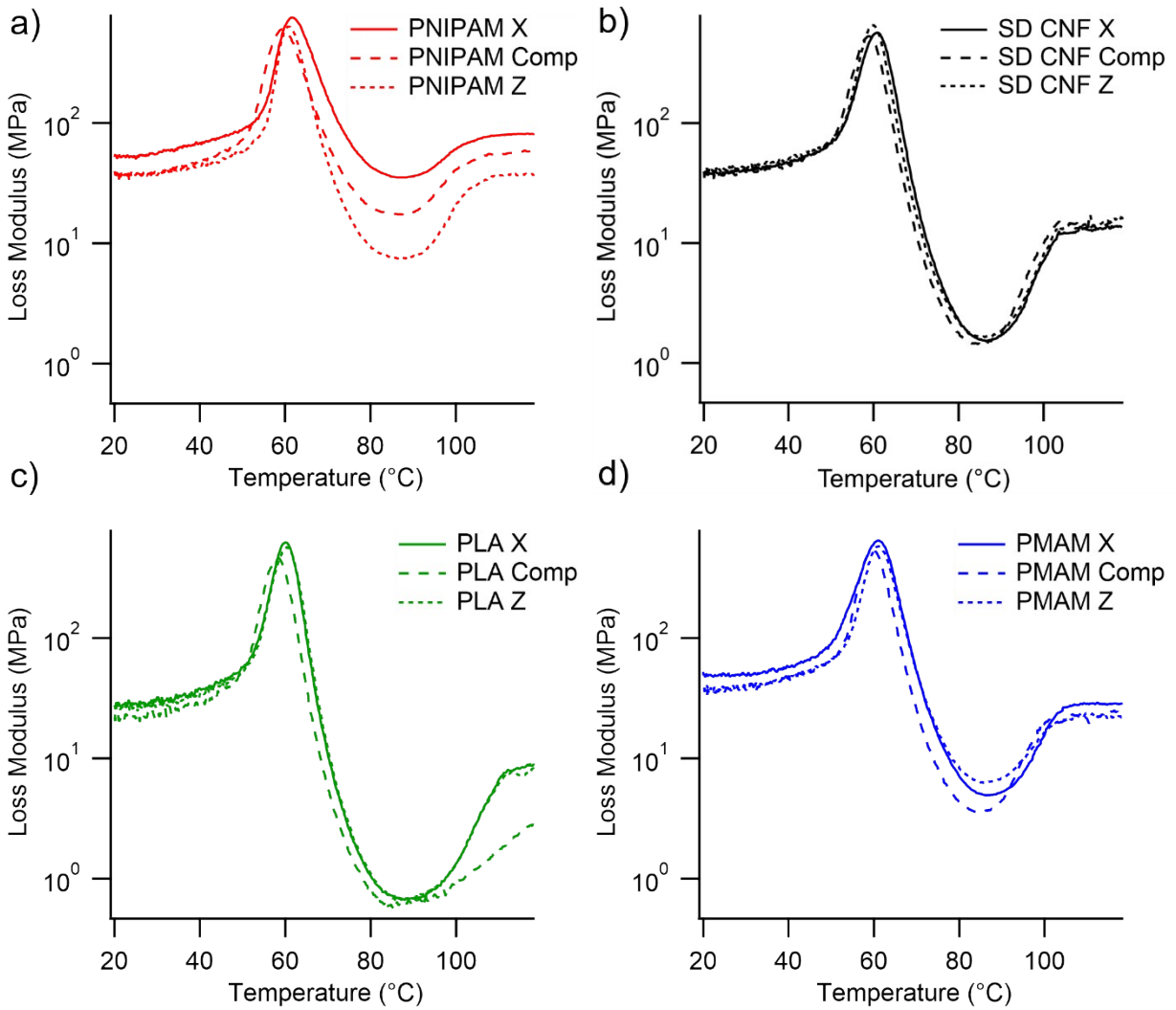


Figure S15. Loss moduli of a) PNIPAM-MetCNF, b) SD CNF, c) neat PLA, and d) PMAM-MetCNF composites in both printing directions and compression molded as a function of temperature measured by DMA.

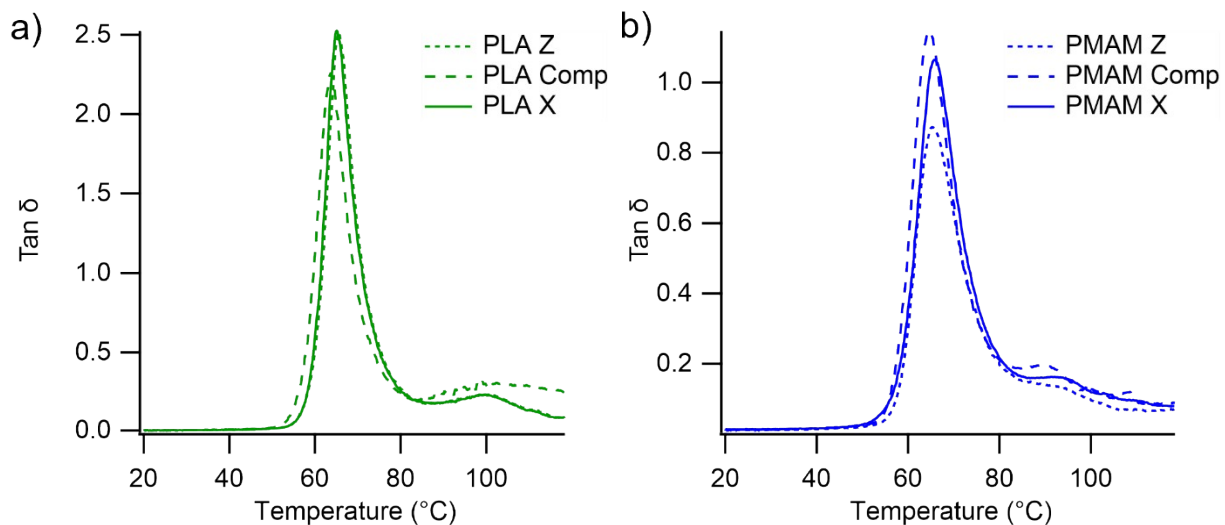


Figure S16. Tan delta of a) neat PLA and b) PMAM-MetCNF composites in both printing directions and compression molded as a function of temperature measured by DMA.

References

- [1] Kelly PV, Cheng P, Gardner DJ, Gramlich WM. Aqueous Polymer Modification of Cellulose Nanofibrils by Grafting-Through a Reactive Methacrylate Group. *Macromol. Rapid Commun* 2021;42(3):2000531.
- [2] Chen SY, Feng Z, Yi X. A general introduction to adjustment for multiple comparisons. *J. Thorac. Dis.* 2017;9(6):1725-1729.
- [3] Oksman K, Skrifvars M, Selin JF. Natural Fibres as Reinforcement in Polylactic Acid (PLA) Composites. *Compos. Sci. Technol* 2003;63:1317-1324.
- [4] Aliotta L, Cinelli P, Coltelli NB, Lazzeri A. Rigid filler toughening in PLA-Calcium Carbonate composites: Effect of particle surface treatment and matrix plasticization. *Eur. Polym. J* 2019;113:78-88.
- [5] Kelly PV, Shams Es-haghi S, Lamm ME, Copenhaver K, Ozcan S, Gardner DJ, Gramlich WM. Polymer-Grafted Cellulose Nanofibrils with Enhanced Interfacial Compatibility for Stronger Poly(lactic acid) Composites. *Appl. Polym. Mater* 2023;5: 3661-3676.

- [6] Androsch R, Schick C, Di Lorenzo ML. Melting of Conformationally Disordered Crystals (α' -Phase) of Poly(l-lactic acid). *Macromolecular Chemistry and Physics* 2014; 215: 1134 – 1139.